Proceedings of the Combustion Institute SAND2020-1232C

Turbulence, evaporation and combustion interactions in n-heptane sprays under high pressure conditions using DNS

--Manuscript Draft--

Manuscript Number:	PROCI-D-19-00961
Article Type:	6. Spray/Droplet/Supercritical Combust.
Keywords:	spray combustion; Auto-ignition; low-temperature chemistry; Direct numerical simulation
Corresponding Author:	Haiou Wang Zhejiang University Hangzhou, CHINA
First Author:	Haiou Wang
Order of Authors:	Haiou Wang
	Kun Luo
	Evatt R. Hawkes
	Jacqueline H. Chen
	Jianren Fan
Abstract:	The evaporation and combustion of n-heptane sprays under high pressure (20 atm) conditions were investigated using three-dimensional direct numerical simulations (DNS) in the present work. Two initial temperatures were considered, i.e. 860 K and 1180 K. Low-temperature combustion, which is controlled by low-temperature chemical pathways, occurs in the 860 K cases while single-stage combustion occurs in the 1180 K cases. Spray evaporation and combustion in isotropic turbulence were considered. The interactions of turbulence, evaporation and combustion in sprays are explored. It was found that turbulence promotes the evaporation process. The temperature and mixture-fraction are negatively correlated after evaporation, which impacts the subsequent ignition process. For both low-temperature and single-stage combustion, ignition occurs in regions with low scalar dissipation rate. Low-temperature ignition first appears in lean mixtures while single-stage ignition in rich mixtures. Ignition kernels evolve into reaction fronts, which propagate towards thermally and compositionally stratified mixture and consumes the remaining fuel. Spontaneous ignition front is dominant in low-temperature combustion while deflagrative front is playing an important role in single-stage combustion. The interactions of turbulence and the reaction front structures are examined. Cylindrical elements are the most probable shape of the reaction front for turbulent spray combustion. The flame normal is misaligned with the vorticity vector for both low-temperature and single-stage combustion, indicating that the vortical structures preferentially locate along the tangential plane of the reaction front.

Turbulence, evaporation and combustion interactions in n-heptane sprays under high pressure conditions using DNS

Haiou Wang[a,*], Kun Luo[a], Evatt R. Hawkes[b,c], Jacqueline H. Chen[d], Jianren Fan[a]

[a] *State Key Laboratory of Clean Energy Utilization, Zhejiang University, Hangzhou 310027, PR China*
[b] *School of Manufacturing and Mechanical Engineering, University of New South Wales, Sydney, NSW, 2052, Australia*
[c] *School of Photovoltaics and Renewable Energy Engineering, University of New South Wales, Sydney, NSW, 2052, Australia*
[d] *Sandia National Laboratories, Livermore, CA 94550, USA*

Abstract

The evaporation and combustion of n-heptane sprays under high pressure (20 atm) conditions were investigated using three-dimensional direct numerical simulations (DNS) in the present work. Two initial temperatures were considered, *i.e.* 860 K and 1180 K. Low-temperature combustion, which is controlled by low-temperature chemical pathways, occurs in the 860 K cases while single-stage combustion occurs in the 1180 K cases. Spray evaporation and combustion in isotropic turbulence were considered. The interactions of turbulence, evaporation and combustion in sprays are explored. It was found that turbulence promotes the evaporation process. The temperature and mixture-fraction are negatively correlated after evaporation, which impacts the subsequent ignition process. For both low-temperature and single-stage

*Corresponding author: Haiou Wang
Email address: wanghaiou@zju.edu.cn (Haiou Wang)

combustion, ignition occurs in regions with low scalar dissipation rate. Low-temperature ignition first appears in lean mixtures while single-stage ignition in rich mixtures. Ignition kernels evolve into reaction fronts, which propagate towards thermally and compositionally stratified mixture and consumes the remaining fuel. Spontaneous ignition front is dominant in low-temperature combustion while deflagrative front is playing an important role in single-stage combustion. The interactions of turbulence and the reaction front structures are examined. Cylindrical elements are the most probable shape of the reaction front for turbulent spray combustion. The flame normal is misaligned with the vorticity vector for both low-temperature and single-stage combustion, indicating that the vortical structures preferentially locate along the tangential plane of the reaction front.
Keywords: Spray combustion, Auto-ignition, Low-temperature chemistry, Direct numerical simulation

1. Introduction

Spray combustion exists in many industrial applications including diesel engines, aircraft engines and gas turbines, which involves complex processes such as turbulence, evaporation, mixing, and chemical reactions. The evaporation and mixing between fuel vapor and oxidizer are considerably affected by turbulence. In practical engines with elevated pressure, complex combustion dynamics interact with turbulence, influencing the characteristics of fuel efficiency and pollutant emission [1, 2]. A better fundamental understanding of turbulence, evaporation and combustion interactions in sprays is required to develop advanced predictive models and to improve designs of practical

combustion devices.

Direct numerical simulation (DNS) is a very useful tool for investigations of spray combustion. It has been employed for spray combustion in two-dimensional (2D) isotropic turbulence/jets [3, 4], and three-dimensional (3D) configurations with simple chemistry [5–8]. Several 3D DNS for spray combustion with detailed chemistry were performed recently [9–12]. For example, Borghesi *et al.* [9] carried out DNS of turbulent $n-$heptane sprays autoigniting at high pressure conditions. It was found that ignition occurred in regions of the most reactive mixture-fraction and low scalar dissipation rate. This work was later extended to a study of autoignition of $n-$heptane sprays in methane/air mixtures [10], relevant to pilot-ignited dual fuel engines. Abdelsamie *et al.* [11] investigated evaporation and autoignition in spatially developing $n-$heptane sprays with high ambient temperatures and a pressure of 5 bar. It is worth noting in these spray DNS studies, the ambient temperature was high and only single-stage ignition was observed.

In practical engines with large hydrocarbon fuels such as $n-$heptane under higher pressure and low temperature conditions, low-temperature combustion, which is controlled by low-temperature chemical pathways [13], might also play an important role. Low-temperature combustion is associated with low heat release rate and a small increase of temperature. It is expected to affect the occurrence of knock in gasoline engines [14] and to assist the stabilization of diesel flames [2]. Low-temperature combustion has been studied with a single droplet [15]. Low-temperature combustion was also found in droplet combustion in microgravity environment, relevant to fire safety in space vehicles [16]. However, there is a gap in understanding of

low-temperature combustion in sprays and its interaction with turbulence.

Ignition in sprays typically occurs in thermally and compositionally stratified mixture attributed to evaporation and evaporative cooling. The effects of thermal and composition stratification on autoignition in stratified charge compression-ignition (SCCI)/HCCI conditions have been studied in 2D DNS [17, 18]. In these studies, the initial distribution of temperature and mixture-fraction was assumed based on spectrum functions. The effects of spray evaporation on the correlation between temperature and mixture-fraction, and the subsequent ignition behavior should be understood.

In the above context, the objective of the present study is three-fold. First, 3D DNS of spray combustion with detailed chemistry under high pressure conditions are performed with different initial temperatures. Low-temperature combustion and single-stage combustion of sprays are investigated. Second, the evaporation and combustion processes in various DNS cases are examined. The effects of turbulence on evaporation, ignition and flame dynamics are explored. Finally, the interactions of turbulence and the reaction front are studied in both low-temperature and single-stage combustion.

2. Computational details

2.1. Governing equations

The DNS code S3D [19] was employed for the simulations. It solves the compressible governing equations of continuity, momentum, total energy and species mass fractions using high-order finite difference methods. The governing equations for the gas phase are provided in the supplementary

material. The liquid phase is modeled using a point-source approach. The droplets are assumed to be spherical and properties of the fuel are uniform inside the droplets. Droplet rotation, distortion and inter-droplet interactions are neglected. The governing equations for the position $\boldsymbol{X}_k$, velocity $\boldsymbol{V}_k$, mass m_k and temperature T_k of the kth droplet are written as:

$$\frac{d\boldsymbol{X}_k}{dt} = \boldsymbol{V}_k \tag{1}$$

$$\frac{d\boldsymbol{V}_k}{dt} = f\frac{\boldsymbol{U}(\boldsymbol{X}_k, t) - \boldsymbol{V}_k}{\tau_p} \tag{2}$$

$$\frac{dm_k}{dt} = -\frac{\mathrm{Sh}}{3\mathrm{Sc_g}}\frac{m_k}{\tau_p}\ln(1+\mathrm{B_M}) \tag{3}$$

$$\frac{dT_k}{dt} = \frac{\mathrm{Nu}}{3\mathrm{Pr_g}}\frac{c_{p,g}}{c_L}\frac{T-T_k}{\tau_p} + \frac{L_{vap}}{m_k c_L}\frac{dm_k}{dt} \tag{4}$$

where $\boldsymbol{U}$ and T are the gas velocity and temperature at the droplet position, respectively, τ_p is the droplet relaxation time, f is a correction to the stokes drag, $\mathrm{Sc_g}$ and $\mathrm{Pr_g}$ are the Schmidt and Prandtl numbers of the gas phase, respectively, Nu and Sh are the corrected Nusselt and Sherwook numbers, respectively, $c_{p,g}$ and c_L are the heat capacity of the gas and liquid phases, respectively, L_{vap} is the latent heat of evaporation, and $\mathrm{B_M}$ is the mass transfer number [7, 20].

Two-way coupling between the gas and liquid phases was considered. The droplet source terms for mass, $\dot{S}_m$, momentum, $\dot{S}_{v_i}$, total energy, $\dot{S}_e$, and species mass fraction, $\dot{S}_{Y_i}$, in the gas phase equations [7, 12] are computed as:

$$\dot{S}_m = -\frac{1}{\Delta V}\sum_k \alpha_k \frac{dm_k}{dt} \tag{5}$$

$$\dot{S}_{v_i} = -\frac{1}{\Delta V}\sum_k \alpha_k \frac{d(m_k v_{k,i})}{dt} \tag{6}$$

$$\dot{S}_e = -\frac{1}{\Delta V}\sum_k \alpha_k \frac{d}{dt}(c_L m_k T_k + \frac{m_k v_{k,i} v_{k,i}}{2}) \tag{7}$$

$$\dot{S}_{Y_i} = -\frac{1}{\Delta V}\sum_k \alpha_k \frac{dm_k}{dt} \text{ for } Y_i = Y_{vapor} \tag{8}$$

where ΔV is the control volume of the node, α_k is distribution coefficient of the kth droplet source term on the node and Y_{vapor} is the mass fraction of vapor.

The performance of the droplet model described above is verified by comparing the predictions of the DNS code and the measurements [21] for a single $n-$heptane droplet. The validation is provided in the supplementary material.

2.2. Chemistry

In the present work, $n-$heptane is used as the fuel. A reduced mechanism involving 58 species and 387 reactions is employed for $n-$heptane combustion [22]. This mechanism has been validated for various problems such as ignition, extinction and flame propagation [22]. The mechanism includes low-temperature chemistry, which enables the study of low-temperature combustion.

2.3. Configuration

The computational domain is a cubic box with 2 mm in each direction. Periodic boundary conditions are used in all directions. Four laminar and turbulent cases are considered as shown in Table 1. The ambient pressure P_0 is 20 atm. The ambient temperature T_0 is 860 K for case A/B, and is 1180 K for case C/D. In the turbulent cases, the initial turbulence field is generated using an isotropic kinetic energy spectrum function by Passot-Pouquet [23].

Table 1: Simulation parameters

case	u' (m/s)	l (mm)	τ_e (ms)	T_0 (K)	ϕ
A	-	-	0.44	860	0.35
B	1.0	0.3	0.44	860	0.35
C	-	-	0.23	1180	0.20
D	1.0	0.3	0.23	1180	0.20

The most energetic turbulence length scale l is 0.3 mm so that there are at least $6l$ in each direction. The turbulent velocity u' is 1.0 m/s, and therefore the turbulent time scale τ_f is 0.3 ms, which is comparable to the evaporation time of the droplets, τ_e.

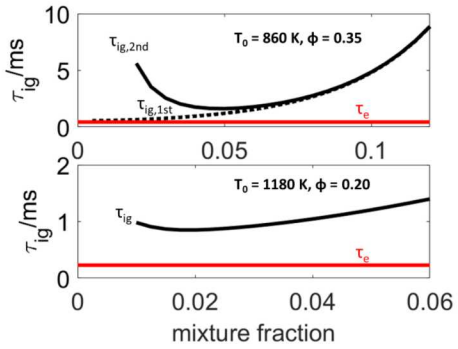

Figure 1: Autoignition time τ_{ig} as a function of the mixture-fraction. The evaporation time τ_e is also superimposed.

Fuel droplets are distributed randomly at the initial time. The initial droplet size D_0 is 15 μm in all cases, the initial droplet temperature is 300 K, and the initial droplet velocity is the same as the flow velocity at the droplet location. Lean combustion is considered. For case A/B with $T_0 = 860$ K, the equivalence ratio ϕ is 0.35, while for case C/D with $T_0 = 1180$ K, the

equivalence ratio ϕ is decreased to 0.2 to avoid high combustion temperature. The parameters are chosen so that two-stage ignition with low-temperature chemistry occurs in case A/B while only single-stage ignition exists in case C/D. Fig. 1 shows the ignition time τ_{ig} as a function of the mixture-fraction (Z) based on adiabatic mixing between the fuel and oxidizer using homogeneous constant-volume reactor simulations. It is seen that when $T_0 = 860$ and $\phi = 0.35$ the first-stage (low-temperature) ignition time increases consistently with Z; the second-stage (high-temperature) ignition time is much larger in the lean region. Therefore, low-temperature combustion and high-temperature combustion are largely separated in the current study. To focus on the behavior of low-temperature combustion, only low-temperature ignition and the subsequent front propagation were simulated for cases A and B with $T_0 = 860$ K and $\phi = 0.35$. Fig. 1 indicates that, when $T_0 = 1180$ K and $\phi = 0.20$, the ignition time is minimum at $Z = 0.02$ and it increases slowly with Z for $Z > 0.02$.

In the present configuration, the ignition time τ_{ig} is longer than the evaporation time τ_e. Therefore, the evaporation and reaction processes are decoupled. The grid resolution is 31 μm during the evaporation phase so that point-particle assumption is valid. After the evaporation is finished, the solution is mapped to fine grids with a resolution of 7.8 μm for the reaction phase to capture the thin reaction zone structure. Turbulence is resolved using both resolutions.

3. Results and discussion

Figures 2a and 2b show the temporal evolutions of volume-averaged mean temperature and species mass fractions. In all cases the temperature first decreases due to evaporative cooling, and then increases when ignition occurs. The evaporation process for the turbulent cases completes earlier than the corresponding laminar cases, which is consistent with previous DNS results [7, 9]. The scatter plots of T and Z right after evaporation are displayed in Figs. 2c and 2d. The variables T and Z are negatively correlated for all cases, which is consistent with the assumption made in previous DNS of SCCI/HCCI studies [17, 18]. Fluctuations of T are also observed in laminar cases, which is due to the weak turbulence generated during the evaporation process.

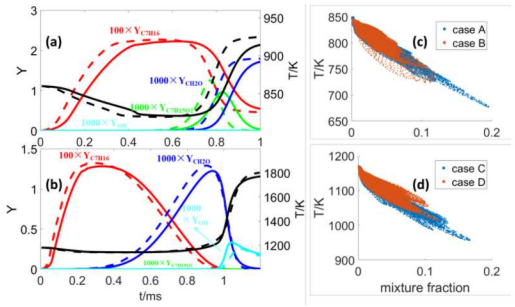

Figure 2: Temporal variations of volume-averaged mean temperature and species mass fractions of C_7H_{16}, $C_7H_{15}O_2$, CH_2O, and OH: (a) case A (solid lines) and case B (dashed lines), and (b) case C (solid lines) and case D (dashed lines). Scatter plots of temperature and mixture-fraction from a representative plane for (c) case A and case B at $t = 0.50$ ms, and (d) case C and case D at $t = 0.25$ ms.

Due to the combined effect of faster evaporation and turbulent mixing, ignition of case B takes place earlier than case A as shown in Fig. 2. Com-

paratively, the ignition of case C and case D occurs at a similar time. It has been shown that alkyl-peroxy (RO_2) could be used as a marker for low-temperature chemistry [13]. Here, $C_7H_{15}O_2$ peaks in the reaction phase and is consumed completely at the end of low-temperature combustion for cases A and B. The radical CH_2O is shown to be one of the main products for low-temperature combustion. On the other hand, $C_7H_{15}O_2$ is absent in cases C and D, where low-temperature chemistry is essentially not activated. The radical CH_2O is accumulated in the induction phase, and is consumed in single-stage combustion for cases C and D.

In the following, the results of low-temperature combustion are first presented in detail, which is followed by the results of single-stage combustion.

3.1. Low-temperature combustion

The process of low-temperature combustion is illustrated in Figs. 3-4. Fig. 3 shows three-dimensional volume renderings of heat release rate at three time instants for cases A and B, while Fig. 4 presents the temperature conditionally averaged on mixture-fraction, correspondingly. It is observed that autoignition firstly occurs in large volumes at $t_1 = 0.74$ ms for case A and $t_1 = 0.69$ ms for case B, with most of the heat release rate found in low mixture-fraction regions, consistent with Fig. 1, which shows that low-temperature ignition time increases with mixture-fraction. Pockets with relatively high heat release rate are also observed, and they are identified as ignition kernels.

Previous studies of single-stage ignition and low-temperature ignition showed that ignition occurs in low scalar dissipation rate regions [18, 24, 25], related to less heat loss during the induction phase. It is of interest to exam-

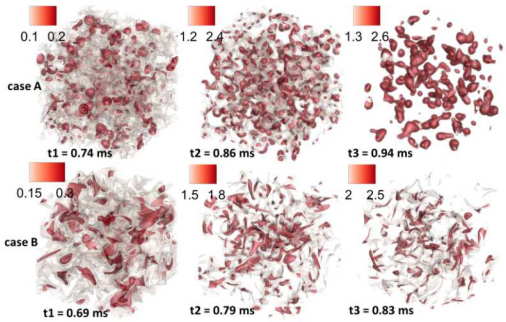

Figure 3: Three-dimensional volume rendering of heat release rate ($\times 10^{10}$ J/m^3·s) for case A and case B at different time instants.

ine how the scalar dissipation rate influences the low-temperature ignition behavior of sprays. Fig. 5 shows the heat release rate doubly conditioned on the scalar dissipation rate and mixture-fraction at $t = t_1$. It is readily observed that most heat is produced in low scalar dissipation rate regions, where low-temperature ignition occurs, consistent with previous findings.

The time instant of $t_2 = 0.86$ ms for case A and $t_2 = 0.79$ ms for case B corresponds to the maximum volume-averaged mean heat release rate during the low-temperature combustion process; the location of high heat release rate is shifted in physical and mixture-fraction space compared to that at $t = t_1$. In Fig. 6, reaction front structures are observed for both cases at $t = t_2$, which could be either spontaneous ignition front or deflagration front [26]. The iso-surface of $Y_{C_7H_{16}} = 0.022$ corresponds well to the maximum heat release rate location, therefore, it is used to denote the reaction front in the following analysis for low-temperature combustion. In order to quantify the relative importance of spontaneous ignition and deflagration fronts, the species budget of CH_2O (an important product of low-temperature combustion) conditioned on distance function, which measures the shortest normal

distance to the reaction front [27], is presented in Fig. 6. It is seen that the reaction term is much larger than the diffusion term in both cases, indicating that spontaneous ignition front prevails in low-temperature combustion.

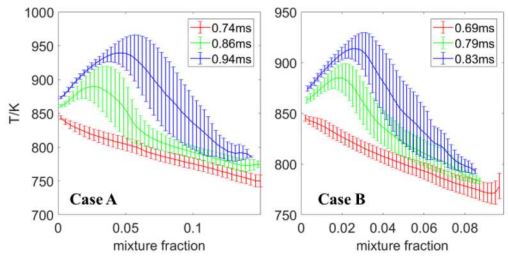

Figure 4: Temperature conditionally averaged on mixture-fraction for case A and case B at various timings. The error bars correspond to the conditional standard deviation.

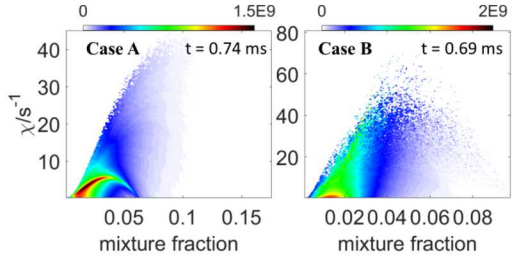

Figure 5: Heat release rate ($J/m^3 \cdot s$) double conditionally averaged on scalar dissipation rate and mixture-fraction at $t = t_2$ for case A and case B.

There are considerable interactions between turbulence and the reaction front, which deserves further investigation. The geometry of the reaction front can be characterized using a shape factor, H_k, which is defined as:

$$H_k = \begin{cases} k_1/k_2 & \text{for } |k_1| \leq |k_2| \\ k_2/k_1 & \text{for } |k_2| < |k_1| \end{cases} \tag{9}$$

where k_1 and k_2 are the two principal curvatures. The shape factor describes the local geometry at each point on the reaction front, *i.e.* H_k = -1 indicates a

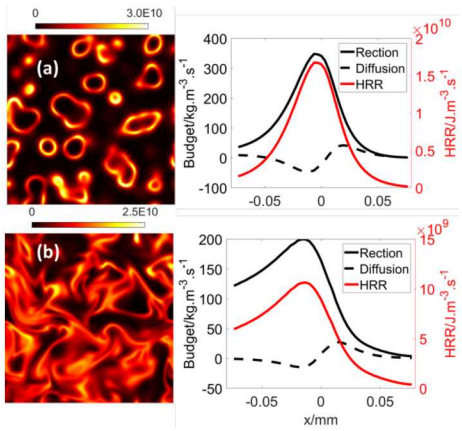

Figure 6: Heat release rate (HRR) distributions in a typical plane and CH_2O budget conditioned on the distance function at $t = t_2$ for (a) case A and (b) case B.

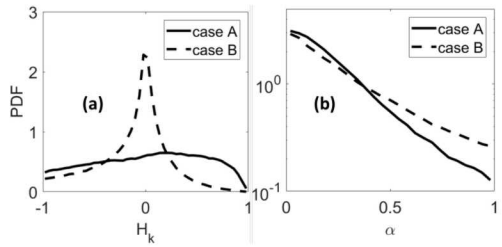

Figure 7: PDFs of (a) the shape factor and (b) the angle between flame normal and vorticity, α, at $t = t_2$. A logarithmic scale is used for the PDF of α to highlight the difference between the two cases.

saddle element, $H_k = 0$ indicates a cylindrical element and $H_k = 1$ indicates a spherical element [28]. Fig. 7a shows the probability density functions (PDFs) of H_k at $t = t_2$. For case A, the most probable value of H_k is positive. However, the PDF at $H_k = 1$ (spherical element) is zero. Note although there is no turbulence in case A at initial time, weak turbulence is generated due to droplet motion, evaporation and chemical reaction, which impacts the reaction front structure so that no value of $H_k = 1$ is observed.

As for case B, the most probable value is at $H_k = 0$ (cylindrical element), and negative values are more likely than positive ones [28].

A variable α is introduced to denote the alignment between the flame normal vector $\mathbf{n}$ and the vorticity vector $\boldsymbol{\omega}$, *i.e.* $\alpha = |\mathbf{n} \cdot \boldsymbol{\omega}|$. The PDFs of α at $t = t_2$ are displayed in Fig. 7b. A logarithmic scale is used for the PDF to highlight the difference between the two cases. It is seen that the most probable value of α is zero for both cases, indicating $\mathbf{n}$ is mainly misaligned with $\boldsymbol{\omega}$. Therefore, turbulence influences the local reaction front structure with the vorticity vector preferentially locating along the tangential plane of the reaction front. A similar trend was observed in premixed jet flames [29].

The time instant of $t_3 = 0.94$ ms for case A and $t_3 = 0.83$ ms for case B corresponds to the end of the low-temperature combustion process. Individual reaction zones are observed at this time, which consume the remaining fuel.

3.2. Single-stage combustion

In this section, the results of single-stage combustion for cases C and D are presented. Some comments are made on the difference between single-stage combustion and low-temperature combustion.

Figure 8 displays three-dimensional volume renderings of heat release rate at three time instants for cases C and D. It is seen that at $t_1 = 0.97$ ms for case C and $t_1 = 0.98$ ms for case D, some ignition kernels with significant heat release rate have developed. In contrast to low-temperature ignition in cases A and B which occurs almost volumetrically (see Fig. 3), single-stage ignition is only found in a few ignition kernels.

Figure 9 shows the temperature conditionally averaged on mixture-fraction

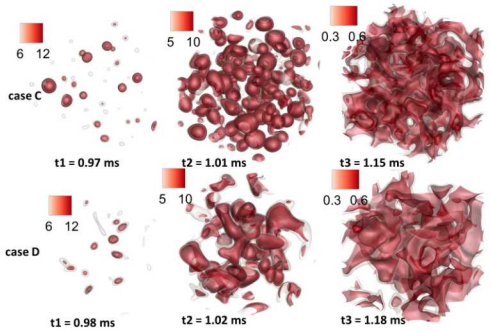

Figure 8: Three-dimensional volume rendering of heat release rate ($\times 10^{10}$ J/m^3·s) for case C and case D at different time instants.

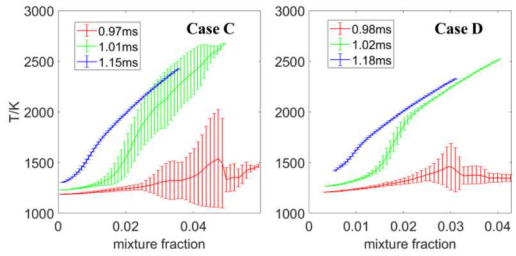

Figure 9: Temperature conditionally averaged on mixture-fraction for case C and case D at various timings. The error bars correspond to the conditional standard deviation.

at the same time instants as in Fig. 8. Large conditional fluctuations are observed in case C. Note that local scalar dissipation rate in the laminar case can vary significantly related to mixture-fraction gradient by evaporation. Ignition occurs in region with $Z > 0.02$ for both cases, while homogeneous reactor simulations indicate the most reactive mixture-fraction should be 0.02. It is worth noting that homogeneous reactor simulations neglect the effects of heat and species mixing, which might be responsible for the discrepancy. Compared to low-temperature ignition, single-stage ignition occurs in richer mixtures. Similar to low-temperature combustion, heat is mainly

generated in low scalar dissipation rate regions during the ignition phase for single-stage combustion (not shown).

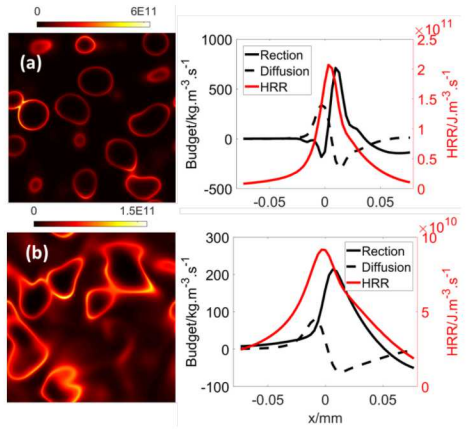

Figure 10: Heat release rate (HRR) distributions in a typical plane and OH budget conditioned on the distance function at $t = t_2$ for (a) case C and (b) case D.

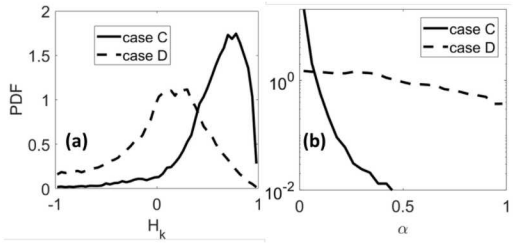

Figure 11: PDFs of (a) the shape factor and (b) the alignment between flame normal and vorticity, α, at $t = t_2$. A logarithmic scale is used for the PDF of α to highlight the difference between the two cases.

At $t_2 = 1.01$ ms for case C and $t_2 = 1.02$ ms for case D, the ignition kernels evolve into thin reaction fronts as demonstrated in Fig. 10. The iso-surface of $T = 1640$ K is found to correlate well the the maximum heat release rate location, which is used to represent the reaction front in the following analysis

for single-stage combustion. Fig. 10 also shows the diffusion and reaction terms of OH (an important product of single-stage combustion) conditioned on the distance function. The two terms are of the same order of magnitude, indicating that deflagrative front propagation is playing an important role for single-stage combustion.

The impact of turbulence on the shape of the reaction front in single-stage combustion is examined in Fig. 11a, which shows the PDFs of H_k at $t = t_2$. Most values of H_k for case C are positive and the most probable value is close to unity, indicating that the local elements of the reaction front are close to spherical, which can also be visualized in Fig. 8. For case D, cylindrical elements ($H_k = 0$) are dominant and negative values of H_k are more likely than positive values. It is concluded that for both low-temperature and single-stage combustion of turbulent sprays, cylindrical elements are the most common shape of the reaction front. Fig. 11b displays the PDFs of α at $t = t_2$. Similar to low-temperature combustion, the flame normal is misaligned with the voticity vector. The misalignment is more notable in case C with the PDF of α at $\alpha = 0$ for case C being one order of magnitude larger than that for case D.

Finally, at $t_3 = 1.15$ ms for case C and $t_3 = 1.18$ ms for case D, the reaction zone shifts to lean regions and the remaining fuel is consumed.

4. Conclusions

In the present work, DNS of $n-$heptane spray combustion under high-pressure conditions were performed without and with initial turbulence. Various DNS spray cases with low-temperature combustion and single-stage com-

bustion are investigated. The interactions of turbulence, evaporation, and combustion characteristics were revealed. The main findings are summarized as follows. *First*, for low-temperature combustion, the evaporation and ignition complete earlier in the turbulent case than the laminar case. The temperature and mixture-fraction are negatively correlated after evaporation, and ignition occurs firstly in lean regions with low scalar dissipation rate. Spontaneous ignition is dominant in the low-temperature combustion process. *Second*, for single-stage combustion, the ignition delays of the laminar and turbulent cases are similar. In contrast to low-temperature ignition, single-stage ignition occurs in rich regions. Thin deflagrative fronts are identified, and the reaction fronts propagate towards lean regions. *Finally*, the interactions of turbulence and reaction fronts were examined. In general, the most probable value of the shape factor H_k is zero and negative values are more likely than positive ones for turbulent cases, while positive H_k values are dominant in laminar cases. The local reaction front is influenced by turbulence so that the flame normal is preferentially misaligned with the vorticity vector for both low-temperature and single-stage combustion.

Acknowledgments

This work was supported by Natural Science Foundation of China (Grant No.: 91841302, 51976185).

References

[1] M. Yao, Z. Zheng, H. Liu. Progress and recent trends in homogeneous charge compression ignition (HCCI) engines. Prog. Energy Combust.

Sci. 35 (2009) 398–437.

[2] M. P. B. Musculus, P. C. Miles, L. M. Pickett. Conceptual models for partially premixed low-temperature diesel combustion. Prog. Energy Combust. Sci. 39 (2013) 246–283.

[3] P. Domingo, L. Vervisch, J. Réveillon. DNS analysis of partially premixed combustion in spray and gaseous turbulent flame-bases stabilized in hot air. Combust. Flame 140 (2005) 172–195.

[4] Y. Wang, C. J. Rutland. Effects of temperature and equivalence ratio on the ignition of n -heptane fuel spray in turbulent flow. Proc. Combust. Inst. 30 (2005) 893–900.

[5] P. Schroll, A. P. Wandel, R. S. Cant, E. Mastorakos. Direct numerical simulations of autoignition in turbulent two-phase flows. Proc. Combust. Inst. 32 (2009) 2275–2282.

[6] K. Luo, H. Pitsch, M. G. Pai, O. Desjardins. Direct numerical simulations and analysis of three-dimensional n -heptane spray flames in a model swirl combustor. Proc. Combust. Inst. 33 (2011) 2143–2152.

[7] H. Wang, K. Luo, J. Fan. Effects of turbulent intensity and droplet diameter on spray combustion using direct numerical simulation. Fuel 121 (2014) 311–318.

[8] T. Kitano, J. Nishio, R. Kurose, S. Komori. Evaporation and combustion of multicomponent fuel droplets. Fuel 136 (2014) 219–225.

[9] G. Borghesi, E. Mastorakos, R. S. Cant. Complex chemistry DNS of n -heptane spray autoignition at high pressure and intermediate temperature conditions. Combust. Flame 160 (2013) 1254–1275.

[10] E. Demosthenous, G. Borghesi, E. Mastorakos, R. Stewart. Direct Numerical Simulations of premixed methane flame initiation by pilot n-heptane spray autoignition. Combust. Flame 163 (2016) 122–137.

[11] A. Abdelsamie, D. Thévenin. On the behavior of spray combustion in a turbulent spatially-evolving jet investigated by direct numerical simulation. Proc. Combust. Inst. 37 (2019) 3373–3382.

[12] J. C. K. Tang, H. Wang, M. Bolla, A. Wehrfritz, E. R. Hawkes. A DNS evaluation of mixing and evaporation models for TPDF modelling of nonpremixed spray flames. Proc. Combust. Inst. 37 (2019) 3363–3372.

[13] P. Zhao, C. K. Law. The role of global and detailed kinetics in the first-stage ignition delay in NTC-affected phenomena. Combust. Flame 160 (2013) 2352–2358.

[14] W. Sun, S. Hee, X. Gou, Y. Ju. ScienceDirect Multi-scale modeling of dynamics and ignition to flame transitions of high pressure stratified n -heptane/toluene mixtures. Proc. Combust. Inst. 35 (2015) 1049–1056.

[15] M. Tanabe, T. Bolik, C. Eigenbrod, H. J. Rath, J. Sato, M. Kono. Spontaneous ignition of liquid droplets from a view of non-homogeneous mixture formation and transient chemical reactions. Proc. Combust. Inst. 26 (1996) 1637–1643.

[16] V. Nayagam, D. L. Dietrich, P. V. Ferkul, M. C. Hicks, F. A. Williams. Can cool flames support quasi-steady alkane droplet burning? Combust. Flame 159 (2012) 3583–3588.

[17] G. Bansal, H. G. Im. Autoignition and front propagation in low temperature combustion engine environments. Combust. Flame 158 (2011) 2105–2112.

[18] M. Talei, E. R. Hawkes. ScienceDirect Ignition in compositionally and thermally stratified n -heptane / air mixtures : A direct numerical simulation study. Proc. Combust. Inst. 35 (2015) 3027–3035.

[19] J. H. Chen, A. Choudhary, B. de Supinski, M. DeVries, E. R. Hawkes, S. Klasky, W. K. Liao, K. L. Ma, J. Mellor-Crummey, N. Podhorszki, R. Sankaran, S. Shende, C. S. Yoo. Terascale direct numerical simulations of turbulent combustion using S3D. Computational Science & Discovery 2 (2009) 015001.

[20] R. S. Miller, K. Harstad, J. Bellan. Evaluation of equilibrium and non-equilibrium evaporation models for many-droplet gas-liquid flow simulations. Int. J. Multiphas. Flow 24 (1998) 1025–1055.

[21] H. Nomura, Y. Ujiie, H. J. Rath, J. Sato, M. Kono. Experimental study on high-pressure droplet evaporation using microgravity conditions. Symp. (Int.) Combust. 26 (1996) 1267–1273.

[22] C. S. Yoo, T. Lu, J. H. Chen, C. K. Law. Direct numerical simulations of ignition of a lean n-heptane/air mixture with temperature inhomo-

geneities at constant volume: Parametric study. Combust. Flame 158 (2011) 1727–1741.

[23] T. Passot, A. Pouquet. Numerical simulation of compressible homogeneous flows in the turbulent regime. J. Fluid Mech. 181 (1987) 441–466.

[24] E. Mastorakos, T. A. Baritaud, T. J. Poinsot. Numerical simulations of autoignition in turbulent mixing flows. Combust. Flame 109 (1997) 198–223.

[25] A. Krisman, E. R. Hawkes, M. Talei, A. Bhagatwala, J. H. Chen. A direct numerical simulation of cool-flame affected autoignition in diesel engine-relevant conditions. Proc. Combust. Inst. 36 (2017) 3567–3575.

[26] J. H. Chen, E. R. Hawkes, R. Sankaran, S. D. Mason, H. G. Im. Direct numerical simulation of ignition front propagation in a constant volume with temperature inhomogeneities I . Fundamental analysis and diagnostics. Combust. Flame 145 (2006) 128–144.

[27] H. Wang, E. Hawkes, J. Chen. A direct numerical simulation study of flame structure and stabilization of an experimental high Ka CH4/air premixed jet flame. Combust. Flame 180 (2017) 110–123.

[28] S. Pope, P. Yeung, S. Girimaji. The curvature of material surfaces in isotropic turbulence. Phys. Fluids A 1 (1989) 2010–2018.

[29] H. Wang, E. Hawkes, J. Chen. Turbulence-flame interactions in DNS of a laboratory high Karlovitz premixed turbulent jet flame. Phys. Fluids 28 (2016) 095107.